THE JOURNAL OF PHYSICAL CHEMISTRY Letters

Letter

pubs.acs.org/JPCL

Topography-Correlated Confocal Raman Microscopy with Cylindrical Vector Beams for Probing Nanoscale Structural Order

Xiao Wang,*[,†] Katharina Broch,[‡] Reinhard Scholz,[§] Frank Schreiber,[‡] Alfred J. Meixner,[†] and Dai Zhang*[,†]

[†]Institute of Physical and Theoretical Chemistry, University of Tübingen, Auf der Morgenstelle 18, 72076 Tübingen, Germany

[‡]Institute of Applied Physics, University of Tübingen, Auf der Morgenstelle 10, 72076 Tübingen, Germany

[§]Institut für Angewandte Photophysik, Technische Universität Dresden, D-01062 Dresden, Germany

Supporting Information

ABSTRACT: Cylindrical vector beams, such as radially or azimuthally polarized doughnut beams, are combined with topography studies of pentacene thin films, allowing us to correlate Raman spectroscopy with intermolecular interactions depending on the particular pentacene polymorph. Polarization-dependent Raman spectra of the C−H bending vibrations are resolved layer by layer within a thin film of ∼20 nm thickness. The variation of the Raman peak positions indicates changes in the molecular orientation and in the local environment at different heights of the pentacene film. With the assistance of a theoretical model based on harmonic oscillator and perturbation theory, our method reveals the local structural order and the polymorph at different locations within the same pentacene thin film, depending mainly on its thickness. In good agreement with the crystallographic structures reported in the literature, our observations demonstrate that the first few monolayers grown in a structure are closer to the thin-film phase, but for larger film thicknesses, the morphology evolves toward the crystal-bulk phase with a larger tilting angle of the pentacene molecules against the substrate normal.

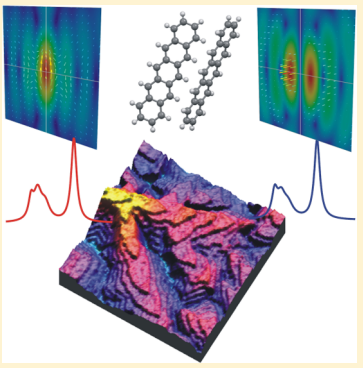

SECTION: Spectroscopy, Photochemistry, and Excited States

Polarized micro-Raman spectroscopy has been intensively applied to investigate the growth and structural evolution of organic semiconductor thin films, such as pentacene, which is one of the promising materials for organic thin-film transistors.[1−6] Its optoelectronic properties depend sensitively on the morphology and crystallinity of the organic films. Polarized micro-Raman spectroscopy has been used to differentiate the thin-film phase and bulk phase of pentacene films.[7−9] These two polymorphs show pronounced differences between their external phonon modes,[10,11] and specific C−H bending modes have been used extensively to identify contributions of different crystal phases to polarized Raman spectra.[10,12] However, when a linearly polarized laser beam is tightly focused as in a micro-Raman experiment, the electric field in the focus distributes not anymore purely parallel to the substrate (*xy* plane), but it has a significant perpendicular component (*z* direction, optical axis of the optical microscope). The depolarization is due to the curvature of the spherical wavefront of the focused field and is predicted to be stronger at high apertures.[13,14] Such a depolarization effect should be carefully considered in terms of retrieving accurate and quantitative molecular information using polarized micro-Raman spectroscopy.

Our research work is aimed at using polarized Raman spectroscopy to distinguish the differences in the local structure even between two adjacent molecular layers within the same pentacene thin films. To accurately quantify such molecular information, we combined cylindrical vector beams, such as a radially or azimuthally polarized doughnut laser beam (RPDB or APDB)[15] with a high numerical aperture (0.998 in air) parabolic mirror to generate in the laser focus either a pure in-plane electric field or a dominant longitudinal electric field component. A sharp gold tip is centered in the mirror focus and kept within a nanometer distance from the surface to probe the topography using shear-force distance control to correlate the polarization-dependent Raman spectra with the local morphology.[16−18] On the basis of the correlated topographic imaging and polarized Raman spectroscopy, we present a highly sensitive polarized Raman spectroscopic method that is able to evaluate the local structural order as well as intermolecular interactions in a pentacene thin film with an average thickness of ∼20 nm.

Figure 1a,b sketches the simulated electric-field distribution (*xy* plane) when a radially (a) or azimuthally (b) polarized laser beam is focused by a parabolic mirror. The arrows represent the directions of the total electric field in the simulated focus plane. Because of the high numerical aperture of the parabolic mirror, the calculated focus of RPDB has a strong longitudinal

Received: January 9, 2014
Accepted: March 6, 2014

   dx.doi.org/10.1021/jz500061y | *J. Phys. Chem. Lett.* 2014, 5, 1048−1054

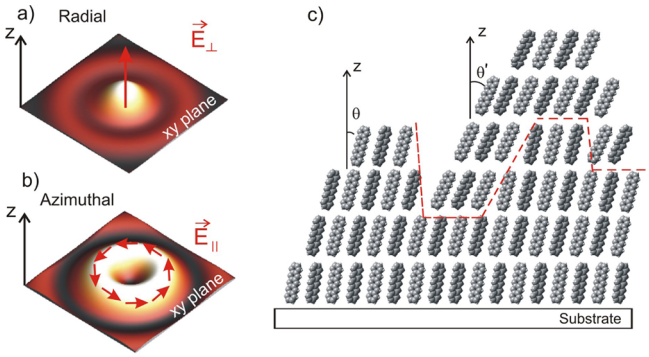

Figure 1. (a,b) Sketches of electric field (E^2) distribution (xy plane) of a radially and an azimuthally polarized laser (632.8 nm) beam focused by a parabolic mirror, respectively. The arrows illustrate the main directions of the electric field in the diffraction limited focal volume. The image sizes are 1 μm × 1 μm. (c) Schematic of polymorphs of pentacene on a Si (100) wafer covered with native oxide layer. θ and θ' represent the different tilting angles of pentacene molecules in different polymorphs with respect to the z axis (normal to the substrate).

component (perpendicular to the substrate surface, $E_\perp$) that is 14.3 times stronger than the transverse mode ($E_\parallel$).[19] In contrast, the focus of APDB has only a transverse field (parallel to the substrate surface, $E_\parallel$).[20,21] On the basis of the distinctive $E_\perp$ and $E_\parallel$ in the focus of RPDB and APDB, the information such as shape, geometry, and orientation of single molecules or nanostructures was deduced from their scattering or photoluminescence (PL) images.[22] In the following discussion, $E_\perp$ will be used to represent the dominant electric-field component in the focus of a RPDB; while $E_\parallel$ will be used to describe the field distribution of a focused APDB.

Pentacene films (20 nm averaged thickness) were grown by organic molecular beam deposition on Si (100) wafers covered with a native oxide layer under ultrahigh vacuum conditions and at a substrate temperature of 300 K.[23] Figure 1c shows the molecular structure of pentacene and the sketched herringbone structure on the substrate.

Figure 2a,b shows confocal optical images of the 30 μm × 30 μm scan area excited by $E_\perp$ and $E_\parallel$, respectively. In the topography image (Figure 2c), randomly distributed pentacene terraces and islands are resolved. These features are about one micrometer wide and several micrometers long. The step between two adjacent terraces is ∼1.6 nm, which is close to the d(001) spacing of thin pentacene films.[24] The branch-like patterns in the optical images originate from these pentacene islands considering their similar shapes and sizes, while the optical contrast is due to the different island heights ("ridges" vs "valleys").

Because the excitation laser line lies in the electronic absorption region of pentacene, both PL and resonant Raman vibrational modes can be well resolved. To compare the optical signal observed from bright and dark areas of the film, four spectra obtained with either $E_\perp$ or $E_\parallel$ are shown in Figure 2d. The locations where the spectra were collected are marked in Figure 2a,b as squares for bright areas and as circles for dark areas. Corresponding to the optical images, the spectra obtained from the bright area show higher PL intensities and stronger superimposed Raman peaks for both laser polarizations. Furthermore, the PL emission maximum is located at ∼1.81 eV (inset, Figure 2d), which is attributed to the fundamental singlet Frenkel exciton of the thin films.[25,26]

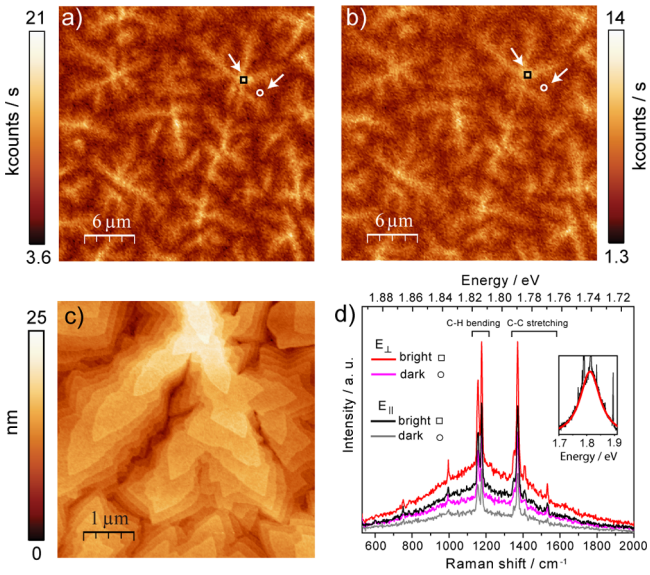

Figure 2. (a,b) Confocal optical images of a pentacene film excited by $E_\perp$ and $E_\parallel$, respectively. (c) Topography image of the pentacene film. (d) PL spectra with superimposed Raman peaks taken from the bright (marked as square) and dark (marked as circle) regions in panels a and b. The inset represents the Gaussian fitting of the PL emission profile. The superimposed sharp lines are the Raman peaks.

The free pentacene molecule has D_{2h} symmetry. Because of the resonant excitation condition, symmetric A_g vibrations are active, which dominate the Raman features appearing in Figure 2d.[8,10,27] The Raman features in the spectral range of 1140−1190 and 1300−1600 cm^{-1} are assigned to C−H bending and C−C stretching modes, respectively. The Raman features of the C−H bending modes at 1158 and 1178 cm^{-1} are related to the motions of H atoms, which are located at both ends and along the sides of the pentacene molecule, respectively. Their intensities and positions are often used to reveal the molecular orientation and structural properties (crystallinity) in the films.[12,28,29]

Figure 3 shows the correlated topography (a) and optical images excited either by $E_\perp$ (b) or $E_\parallel$ (c) that are taken from the same area (5 μm × 5 μm) of the pentacene thin film. One clearly sees the direct correlation of the branch-like patterns in the optical images and the topographically resolved pentacene islands. Numbers marked in Figure 3a represent the positions at which Raman spectra were measured: P1 for the highest position and P15 for the lowest position. The relative heights of all 15 positions are listed in Figure 3f. The error bars indicate the slight height variations of the film within the focal volume of confocal microscopy.[15] Figure 3d,e shows 15 Raman spectra collected from positions P1 to P15, which are normalized to the intensity of the 1178 cm^{-1} peak. The most dramatic spectral differences appear at about 1155 (denoted as ν_1) and 1158 cm^{-1} (denoted as ν_2), where their relative intensity ratios gradually change with the height when excited by $E_\perp$. However, there is less change in the ratio of the intensities of ν_1 and ν_2 when the film is excited by $E_\parallel$. Furthermore, the separation between ν_1 and ν_2 is slightly (∼0.5 cm^{-1}) smaller at topographically lower locations (P12 to P15) than those of higher locations.

The appearances of the two Raman peaks ν_1 and ν_2 are due to the splitting of the vibronic levels, which is caused by the interaction of two inequivalent pentacene molecules in a unit

dx.doi.org/10.1021/jz500061y | J. Phys. Chem. Lett. 2014, 5, 1048−1054

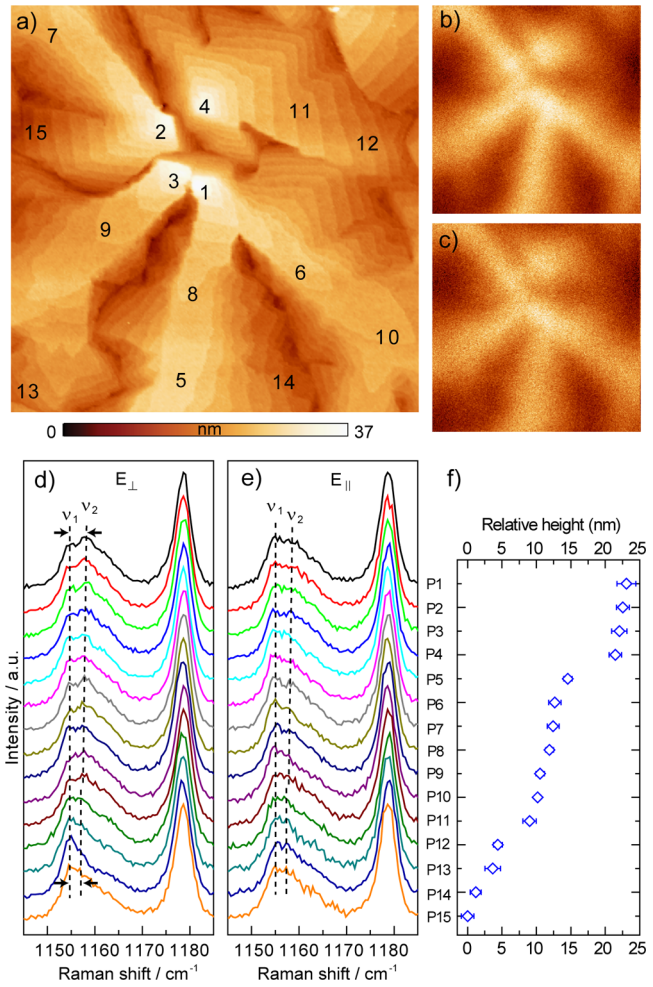

Figure 3. (a–c) Correlated topography and optical images of a pentacene film. Optical images (b) and (c) were obtained by $E_{\perp}$ and $E_{\parallel}$, respectively. Image size: 5 μm × 5 μm. Numbers 1–15 marked in panel a indicate the positions where the spectra were collected. (d,e) Normalized Raman spectra of all positions obtained under $E_{\perp}$ and $E_{\parallel}$ excitation, respectively. The dashed lines are guides to the eye. (f) Relative heights for all 15 positions. The height values are derived from the topography shown in panel a. The lowest position P15 is defined as the reference zero height, and heights of other positions are offset to it.

cell. In molecular crystals, the phenomenon of electronic or vibrational band splitting due to the presence of more than one molecule in the unit cell is called Davydov splitting.[30] By Raman and infrared spectroscopy, the vibrational Davydov splitting of other organic molecular films has been studied.[31−35] By absorption spectroscopy, the electronic Davydov splitting of crystalline oligoacenes has been discussed and interpreted by quantum-chemical calculations.[36−39] It should be noted that the Davydov splitting is still a matter of research and may occur in different ways, for example, Frenkel exciton coupling[39] and admixture of charge-transfer excitations into the lowest singlet excited states.[40] In Figure 3d the peak position of ν_1 stays constant, while the peak position of ν_2 is slightly blue-shifted for thicker films, giving rise to the increasing frequency splitting. The frequency splitting $\Delta\nu$ between ν_1 and ν_2 is ∼3.0 cm^{-1} at P1, while it is ∼2.5 cm^{-1} at P15. It is known that different polymorphs exist in pentacene films. During evolution from monolayer to thicker film, the structure changes from the orthorhombic phase to the thin-film phase and the triclinic bulk phase.[5,24,41−43] The frequency splitting $\Delta\nu$ of the two Raman peaks is relevant to the polymorph. For instance, Cheng et al. have reported an increased Raman frequency splitting from about 2.51 to 3.60 cm^{-1} when the averaged film thickness increases from 5 to 300 nm.[8] Herein, by sensitive visualization of Raman frequency splitting and intensity variation, we demonstrate different polymorphs in subsequent molecular layers within one molecular island.

Besides the peak (ν_1 and ν_2) separation, the changes of the peak intensities at different positions and for the two different polarization states of the probing field are also important to probe the structure of the films. We show in Figure 4a the

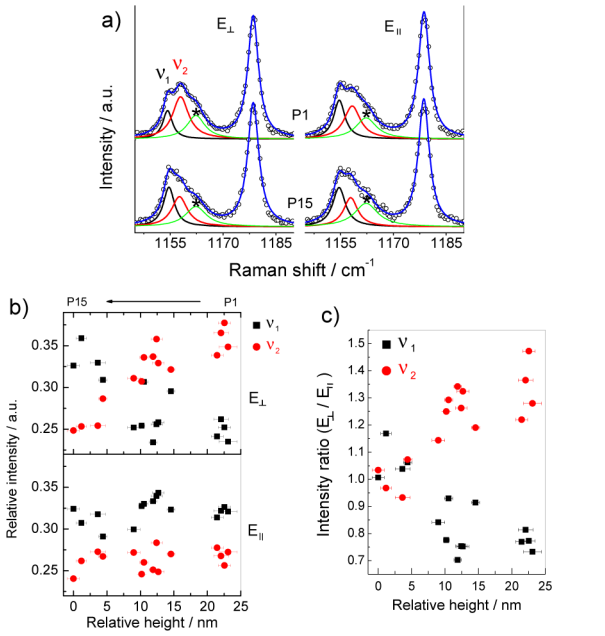

Figure 4. (a) Raman spectra and their fitting curves of the pentacene film at P1 and P15 with $E_{\perp}$ and $E_{\parallel}$, respectively. (b) Peak intensities of Raman modes ν_1 and ν_2 at different heights and polarizations. (c) Relation between the relative heights of the positions and the intensity ratios ($I_{E_{\perp}}/I_{E_{\parallel}}$) for Raman bands ν_1 and ν_2.

Raman spectra and their Lorentzian fitting curves of positions P1 and P15. The blue curves show the overall fitting profiles. The original spectrum data points are indicated as open circles. The black and red curves represent the Raman peaks of ν_1 and ν_2; while the green curve (marked by asterisk) indicates the peak at ∼1162 cm^{-1}, which is another C–H bending mode. In all 15 positions, the peak at 1162 cm^{-1} shows less change than ν_1 and ν_2.

Figure 4b plots the intensity of ν_1 and ν_2 at different heights and polarization conditions, respectively. As shown in the lower panel of Figure 4b, excited by $E_{\parallel}$, ν_1 is stronger than ν_2 at all heights. In contrast, excited by $E_{\perp}$, the intensity of ν_1 (I_{ν_1}) is only stronger than that of ν_2 (I_{ν_1}) at very thin-film positions (P15–P12). If the film is thicker (P11 to P1), I_{ν_1} decreases while I_{ν_2} increases (upper panel, Figure 4b). At the highest position P1, I_{ν_2} is ∼40% higher than I_{ν_1}. Obviously the vibrational motions of ν_1 and ν_2 have different polarization characteristics depending on the film thickness. Figure 4c illustrates such a trend more clearly by comparing the intensity ratios ($I_{E_{\perp}}/I_{E_{\parallel}}$) of ν_1 and ν_2. At topographically low positions

dx.doi.org/10.1021/jz500061y | J. Phys. Chem. Lett. 2014, 5, 1048−1054

(P12−P15), the intensities of ν_1 and ν_2 differ much less when the excitation changes from $E_\perp$ to $E_\parallel$. However, at topographically higher positions (especially P1−P4), dramatic changes in the peak intensity are observed.

The intensities of Raman peaks are influenced by the orientation of the transition dipole moment between the highest occupied molecular orbital (HOMO) and lowest unoccupied molecular orbital (LUMO) transition of the pentacene molecule relative to the exciting electric field. The HOMO−LUMO transition dipole of pentacene is oriented along the short molecular axis (SMA).[23] On the basis of the crystallographic information taken from refs 44 and 45, the crystal structures of the thin film and bulk phase as well as the corresponding tilting of the SMAs are shown in Figure 5. The

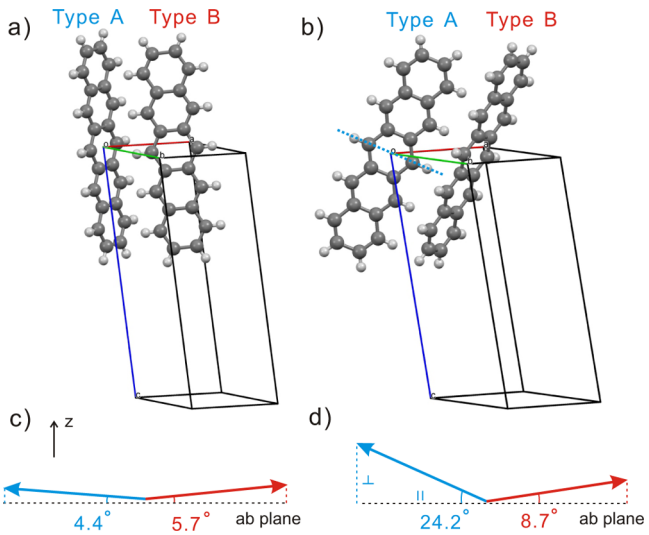

Figure 5. (a,b) Views of two types of pentacene molecules in one unit cell of thin-film phase (d_{001} = 15.4 Å) and bulk phase (d_{001} = 14.1 Å). The blue dotted line indicates the short molecular axis. (c,d) Illustrations of the tilting angles of the SMAs of types A and B of pentacene molecules in the thin film phase and bulk phase. The z axis is perpendicular to the ab plane (substrate plane).

two pentacene molecules in a unit cell are differentiated as the type A and B molecules, which correspond to their center of mass at the unit cell coordinates (0, 0, 0) and (1/2, 1/2, 0), respectively. On the basis of the coordinates of all the atoms, the tilting angle of the molecule axis can be evaluated. For the thin-film phase (d_{001} = 15.4 Å; a = 5.958 Å, b = 7.596 Å, c = 15.6096 Å; α = 81.25°, β = 86.56°, γ = 89.80°) shown in Figure 5a, the tilting angles (with respect to the ab plane) of the SMAs of type A and B molecules are 4.4 and 5.7°, respectively. For the bulk phase (d_{001} = 14.1 Å; a = 6.266 Å, b = 7.775 Å, c = 14.530 Å; α = 76.475°, β = 87.682°, γ = 84.684°) shown in Figure 5b, the tilting angles of the SMAs of type A and B molecules are 24.2 and 8.7°, respectively. Figure 5c,d illustrates the tilting of SMA of type A and B pentacene molecules in the two polymorphs. Although there are at least four different polymorphs reported for pentacene, which probably coexist in pentacene films of different thickness, we consider for simplicity the crystal structures shown in Figure 5a,b as the structure of the topographic low and high locations in the film, respectively.

To understand the frequency splitting and the polarization dependency of ν_1 and ν_2, we performed the following analysis. In the thin-film phase of pentacene,[45] both basis (A and B) molecules in the unit cell interact only weakly so that the rectangular geometry of a free pentacene molecule is essentially conserved. Only one set of four equivalent C−C bonds shows a significant distortion from the full rectangular symmetry D_{2h} so that two of these bonds are compressed by more than 2%. Including some smaller distortions, the overall deformation patterns of both basis molecules from a rectangular shape are nearly identical.

Therefore, the vibrational modes of both basis molecules should remain similar, and their interaction via small mode-specific intermolecular matrix elements should result in a symmetric splitting. In terms of the interaction between classical harmonic oscillators, this can be described by an unperturbed starting Hamiltonian $H_0 = ((p_A^2/2m) + (m/2)\Omega_0^2 x_A^2) + ((p_B^2/2m) + (m/2)\Omega_0^2 x_B^2)$, where the frequencies of the oscillators in both basis molecules A and B coincide, $\Omega_{A,B} = \Omega_0$. The coupling between degenerate mode pairs occurs via a perturbation $H_1 = (m/2)\Delta^2(x_A - x_B)^2$, where breathing modes of the two basis molecules interact only via rather weak quadrupole−quadrupole interactions producing small values of Δ^2. From straightforward analysis of the classical equations of motion, it can be shown that the squared eigenfrequencies are obtained from a diagonalization of the matrix $\begin{pmatrix} \Omega_0^2 + \Delta^2 & \Delta^2 \\ \Delta^2 & \Omega_0^2 + \Delta^2 \end{pmatrix}$ with the solutions

$$\omega_1^2 = \Omega_0^2;\ \ \omega_2^2 = \Omega_0^2 + 2\Delta^2 \tag{1}$$

The crystal bulk phase of pentacene behaves completely differently. One of the basis molecules shows a geometry resembling the thin-film phase; that is, the main deviation from a rectangular shape concerns a compression of two out of the four equivalent longest bonds in the carbon network, again by ∼2%. However, the embedding into the more densely packed crystal phase of pentacene induces a significant compression of C−C bonds parallel to the short axis, with an average of 1.2%. This corresponds to the B basis molecule.

In stark contrast with this behavior remaining rather close to a free molecule, the second basis molecule A is significantly deformed with respect to free pentacene: Within several sets of four equivalent internal C−C bonds, the embedding crystal induces significant distortions so that the deviation from a rectangular shape is about six times larger than that for the basis molecule B.

Hence, even assuming vanishing intermolecular interactions for a specific vibrational mode, the significant internal distortion of the basis molecule A and the compression of the basis molecule B along the short axis are expected to produce slightly modified vibrational frequencies. Therefore, the starting Hamiltonian H_0 for the crystal phase of pentacene already contains different molecular frequencies Ω_A and Ω_B, $H_0 = ((p_A^2/2m) + (m/2)\Omega_A^2 x_A^2) + ((p_B^2/2m) + (m/2)\Omega_B^2 x_B^2)$, where it is reasonable to assume that the more distorted basis molecule A has a higher frequency, $\Omega_A > \Omega_B$. The Davydov splitting occurs again via the intermolecular interaction, parametrized as $H_1 = (m/2)\Delta'^2(x_A - x_B)^2$, where the interaction parameter Δ' in the crystal-bulk phase is expected to remain in the same range as the value Δ in the thin-film phase. The squared eigenfrequencies in the crystal phase can be obtained from a diagonalization of the matrix $\begin{pmatrix} \Omega_A^2 + \Delta'^2 & \Delta'^2 \\ \Delta'^2 & \Omega_B^2 + \Delta'^2 \end{pmatrix}$ with the solutions

dx.doi.org/10.1021/jz500061y | J. Phys. Chem. Lett. 2014, 5, 1048−1054

$$(\omega^2)_{1,2} = \left(\frac{\Omega_A^2 + \Omega_B^2}{2} + \Delta'^2\right) \mp \sqrt{\left(\frac{\Omega_A^2 - \Omega_B^2}{2}\right)^2 + \Delta'^4} \quad (2)$$

The measured Raman signals for the thinnest film (P15 in Figure 3) allow us to determine the parameters for the thin-film phase according to equation (eq 1). Assigning mode positions in terms of wavenumbers, Ω_0 corresponds to 1155 cm^{-1} and Δ to 54 cm^{-1}. For the measurement obtained in the thickest region (P1 in Figure 3), we assume that the interaction parameter Δ' still coincides with the value Δ for the thin-film phase. On this basis, substituting the measured positions of 1155 cm^{-1} for the lower mode (ω_1) and 1158 cm^{-1} for the higher mode (ω_2) into eq 2 yields a value of 1154.4 cm^{-1} to Ω_B and 1156.1 cm^{-1} to Ω_A, corresponding to a splitting of 1.7 cm^{-1} arising from the different geometries of the two basis molecules. The mode splitting is still dominated by the contribution Δ'^4 corresponding to 70% of the argument of the square root in eq 2. Both in the thin-film phase and in the crystal-bulk phase, the polarization dependence of optical spectra in resonance with the HOMO−LUMO transition depends on the orientation of the short axes of the basis molecules with respect to the *ab* plane aligned parallel to the substrate surface.

As previously discussed, in the thin-film phase, both basis molecules have essentially equivalent geometries, involving similar small deviations from a rectangular shape. The HOMO−LUMO transition dipole moments oriented along the short axes of the two basis molecules are tilted by similar angles of 4.4 and 5.7°, with respect to the *ab* lattice plane, coinciding with the substrate orientation. The analysis of the Davydov splitting between the crystal modes in the thin-film phase has started from degenerate molecular vibrations, so that the crystal eigenvectors project as $(1/\sqrt{2}, 1/\sqrt{2})$ and $(-1/\sqrt{2}, 1/\sqrt{2})$ onto the vibrations of the basis molecules. Both of these eigenvectors produce contributions of 50% on each basis molecule. Together with the similar orientation of both basis molecules in the crystal unit cell, a pronounced polarization dependence of the crystal modes ω_1 and ω_2 cannot be expected, in agreement with the vanishing polarization dependence of the spectra taken at P15 in Figure 3.

In the crystal-bulk phase of pentacene, the short axis of the basis molecule *B* is tilted by 8.7° against the *ab* lattice plane, whereas the *A* molecule has a much larger tilting angle of 24.2°. The two long axes of the basis molecules are nearly parallel, so that both are tilted against the substrate normal by ∼25°.The vibrational eigenvectors obtained from the diagonalization give two crystal modes with different weights on the two basis molecules. The lower mode at 1155 cm^{-1} carries a weight of 78% on *B* and of 22% on *A*, whereas the higher mode at 1158 cm^{-1} shows the complementary contributions of 22% on *B* and 78% on *A*.

The larger starting frequency Ω_A together with the stronger tilting of the HOMO−LUMO transition dipole of this basis molecule and the predominant *A* character of the higher crystal mode ω_2 should result in a better visibility in the Raman spectra obtained for an excitation field $E_\perp$ along the substrate normal. This corresponds precisely to our experimental results (Figures 3d and 4b (upper panel)): With radially polarized light giving an electric field $E_\perp$ along the substrate normal in the focus, the relative Raman intensity of ν_2 becomes most prominent.

For polarization $E_\parallel$ parallel to the substrate, no significant polarization dependence of the crystal modes has to be expected because both basis molecules have similar projections of their transition dipoles into the substrate plane, corresponding to cos 8.7° = 0.99 for basis molecule *B* and cos 24.2° = 0.91 for basis molecule *A*. This difference seems to be too small to be resolved with our experimental setup (Figures 3e and 4b (lower panel)): with polarization $E_\parallel$, the observed ratio of the Raman intensities of the crystal modes ν_1 and ν_2 does not depend significantly on film thickness.

The previous reasoning was based on the simplifying assumption that the interaction parameter Δ' in the crystal-bulk phase was in the same range as the value Δ in the thin-film phase. Even if this premise would be released, there is clear evidence that a parametrization of the crystal-bulk phase would still require blue-shifted starting frequencies Ω_A and Ω_B resulting from the more strongly strained starting geometries. Hence, accounting for the different shapes of the two basis molecules, it is completely natural to assume different shifts for the respective vibrational modes. Even a small discrepancy is sufficient for arriving at vibrational eigenvectors of the bulk crystal with different weights on the two basis molecules, so that the eigenvector dominated by the more strained and more tilted basis molecule *A* can produce a pronounced polarization dependence of the Raman intensity, as observed.

In summary, we observed layer-by-layer changes in the Raman shift and intensity of the C−H bending vibrations (ν_1 and ν_2) of pentacene molecules in a 20 nm thick polycrystalline film. We showed that polarization-dependent and diffraction-limited confocal Raman microscopy correlated with nanometer-resolved topography can reveal fine details on the polymorphs and molecular orientation in the pentacene films. During the film evolution, the packing of the pentacene molecules changes from thin-film phase to bulk phase. Because of the more significant inequivalence of basis molecules, we observed a larger frequency splitting of ν_1 and ν_2 at locations with a higher film thickness. Compared with the relatively small tilting angles (4.4 and 5.7° with respect to the *ab* plane) of the SMAs of basis molecules in thin-film phase, one of the basis molecules in the bulk phase shows a significantly large tilting angle (24.2°). Under $E_\perp$ excitation, we observed the increased intensity of peak ν_2 from topographically lower to higher locations due to the increased tilting angles of SMAs. Using such topography combined polarized Raman spectroscopy method, one can sensitively identify the polymorphs, the molecule orientations, and the intermolecular interactions even in one thin pentacene film.

■ ASSOCIATED CONTENT

Ⓢ Supporting Information

Detailed description of the optical confocal microscope and the combined scanning probe microscope and the reproducibility of the results across the sample. This material is available free of charge via the Internet at http://pubs.acs.org.

■ AUTHOR INFORMATION

Corresponding Authors

*E-mail: xiao.wang@uni-tuebingen.de (X.W.).
*E-mail: dai.zhang@uni-tuebingen.de (D.Z.).

Notes

The authors declare no competing financial interest.

■ ACKNOWLEDGMENTS

This research work was supported by the Projektförderung für Nachwuchswissenschaftler/Innen Uni-Tübingen, the DFG (grant ME1600/5-2), the Studienstiftung des deutschen Volkes, and the Landesstiftung Baden-Württemberg (Organische Photovoltaik). We thank Dr. Hans-Georg Mack for computing the pentacene Raman vibrational modes.

■ REFERENCES

(1) Brütting, W.; Adachi, C. *Physics of Organic Semiconductors*; VCH-Wiley: Weinheim, Germany, 2012.
(2) Horowitz, G. Organic Field-Effect Transistors. *Adv. Mater.* **1998**, *10*, 365−377.
(3) Dimitrakopoulos, C. D.; Malenfant, P. R. L. Organic Thin Film Transistors for Large Area Electronics. *Adv. Mater.* **2002**, *14*, 99−117.
(4) Hinderhofer, A.; Schreiber, F. Organic-Organic Heterostructures: Concepts and Applications. *ChemPhysChem* **2012**, *13*, 628−643.
(5) Mattheus, C. C.; Dros, A. B.; Baas, J.; Oostergetel, G. T.; Meetsma, A.; de Boer, J. L.; Palstra, T. T. M. Identification of Polymorphs of Pentacene. *Synth. Met.* **2003**, *138*, 475−481.
(6) Ruiz, R.; Mayer, A. C.; Malliaras, G. G.; Nickel, B.; Scoles, G.; Kazimirov, A.; Kim, H.; Headrick, R. L.; Islam, Z. Structure of Pentacene Thin Films. *Appl. Phys. Lett.* **2004**, *85*, 4926−4928.
(7) Cheng, H. L.; Chou, W. Y.; Kuo, C. W.; Tang, F. C.; Wang, Y. W. Electric Field-induced Structural Changes in Pentacene-based Organic Thin-film Transistors Studied by in Situ Micro-Raman Spectroscopy. *Appl. Phys. Lett.* **2006**, *88*, 161918.
(8) Cheng, H. L.; Mai, Y. S.; Chou, W. Y.; Chang, L. R.; Liang, X. W. Thickness-dependent Structural Evolutions and Growth Models in Relation to Carrier Transport Properties in Polycrystalline Pentacene Thin Films. *Adv. Funct. Mater.* **2007**, *17*, 3639−3649.
(9) Seto, K.; Furukawa, Y. Study on Solid Structure of Pentacene Thin Films Using Raman Imaging. *J. Raman Spectrosc.* **2012**, *43*, 2015−2019.
(10) Brillante, A.; Della Valle, R. G.; Farina, L.; Girlando, A.; Masino, M.; Venuti, E. Raman Phonon Spectra of Pentacene Polymorphs. *Chem. Phys. Lett.* **2002**, *357*, 32−36.
(11) Venuti, E.; Della Valle, R. G.; Brillante, A.; Masino, M.; Girlando, A. Probing Pentacene Polymorphs by Lattice Dynamics Calculations. *J. Am. Chem. Soc.* **2002**, *124*, 2128−2129.
(12) He, R.; Dujovne, I.; Chen, L. W.; Miao, Q.; Hirjibehedin, C. F.; Pinczuk, A.; Nuckolls, C.; Kloc, C.; Ron, A. Resonant Raman Scattering in Nanoscale Pentacene Films. *Appl. Phys. Lett.* **2004**, *84*, 987−989.
(13) Richards, B.; Wolf, E. Electromagnetic Diffraction in Optical Systems. II. Structure of the Image Field in an Aplanatic System. *Proc. R. Soc. London, Ser. A* **1959**, *253*, 358.
(14) Bahlmann, K.; Hell, S. W. Electric Field Depolarization in High Aperture Focusing with Emphasis on Annular Apertures. *J. Microsc.* **2000**, *200*, 59−67.
(15) Stadler, J.; Stanciu, C.; Stupperich, C.; Meixner, A. J. Tighter Focusing with a Parabolic Mirror. *Opt. Lett.* **2008**, *33*, 681−683.
(16) Karrai, K.; Grober, R. D. Piezoelectric Tip-Sample Distance Control for Near-Field Optical Microscopes. *Appl. Phys. Lett.* **1995**, *66*, 1842−1844.
(17) Wang, X.; Zhang, D.; Braun, K.; Egelhaaf, H. J.; Brabec, C. J.; Meixner, A. J. High-Resolution Spectroscopic Mapping of the Chemical Contrast from Nanometer Domains in P3HT:PCBM Organic Blend Films for Solar-Cell Applications. *Adv. Funct. Mater.* **2010**, *20*, 492−499.
(18) Wang, X.; Azimi, H.; Mack, H. G.; Morana, M.; Egelhaaf, H. J.; Meixner, A. J.; Zhang, D. Probing the Nanoscale Phase Separation and Photophysics Properties of Low-Bandgap Polymer: Fullerene Blend Film by Near-Field Spectroscopic Mapping. *Small* **2011**, *7*, 2793−2800.
(19) Zhang, D.; Wang, X.; Braun, K.; Egelhaaf, H. J.; Fleischer, M.; Hennemann, L.; Hintz, H.; Stanciu, C.; Brabec, C. J.; Kern, D. P.; et al. Parabolic Mirror-assisted Tip-enhanced Spectroscopic Imaging for Non-transparent Materials. *J. Raman Spectrosc.* **2009**, *40*, 1371−1376.
(20) Lieb, M. A.; Meixner, A. J. A High Numerical Aperture Parabolic Mirror as Imaging Device for Confocal Microscopy. *Opt. Express* **2001**, *8*, 458−474.
(21) Zhang, D.; Heinemeyer, U.; Stanciu, C.; Sackrow, M.; Braun, K.; Hennemann, L. E.; Wang, X.; Scholz, R.; Schreiber, F.; Meixner, A. J. Nanoscale Spectroscopic Imaging of Organic Semiconductor Films by Plasmon-Polariton Coupling. *Phys. Rev. Lett.* **2010**, *104*, 056601.
(22) Züchner, T.; Failla, A. V.; Meixner, A. J. Light Microscopy with Doughnut Modes: A Concept to Detect, Characterize, and Manipulate Individual Nanoobjects. *Angew. Chem., Int. Ed.* **2011**, *50*, 5274−5293.
(23) Hinderhofer, A.; Heinemeyer, U.; Gerlach, A.; Kowarik, S.; Jacobs, R. M. J.; Sakamoto, Y.; Suzuki, T.; Schreiber, F. Optical Properties of Pentacene and Perfluoropentacene Thin Films. *J. Chem. Phys.* **2007**, *127*, 194705.
(24) Mattheus, C. C.; de Wijs, G. A.; de Groot, R. A.; Palstra, T. T. M. Modeling the Polymorphism of Pentacene. *J. Am. Chem. Soc.* **2003**, *125*, 6323−6330.
(25) Aoki-Matsumoto, T.; Furuta, K.; Yamada, T.; Moriya, H.; Mizuno, K.; Matsui, A. H. Excitonic Photoluminescence in Pentacene Single Crystal. *Int. J. Mod. Phys. B* **2001**, *15*, 3753−3756.
(26) He, R.; Tassi, N. G.; Blanchet, G. B.; Pinczuk, A. Fundamental Optical Recombination in Pentacene Clusters and Ultrathin Films. *Appl. Phys. Lett.* **2005**, *87*, 103107.
(27) Yamakita, Y.; Kimura, J.; Ohno, K. Molecular Vibrations of n Oligoacenes (n=2−5 and 10) and Phonon Dispersion Relations of Polyacene. *J. Chem. Phys.* **2007**, *126*, 064904.
(28) Jentzsch, T.; Juepner, H. J.; Brzezinka, K. W.; Lau, A. Efficiency of Optical Second Harmonic Generation from Pentacene Films of Different Morphology and Structure. *Thin Solid Films* **1998**, *315*, 273−280.
(29) Stenger, I.; Frigout, A.; Tondelier, D.; Geffroy, B.; Ossikovski, R.; Bonnassieux, Y. Polarized Micro-Raman Spectroscopy Study of Pentacene Thin Films. *Appl. Phys. Lett.* **2009**, *94*, 133301.
(30) Davydov, A. S. *Theory of Molecular Excitons*; McGraw-Hill, New York, 1971.
(31) Scholz, R.; Kobitski, A. Y.; Kampen, T. U.; Schreiber, M.; Zahn, D. R. T.; Jungnickel, G.; Elstner, M.; Sternberg, M.; Frauenheim, T. Resonant Raman Spectroscopy of 3,4,9,10-Perylene-Tetracarboxylic-Dianhydride Epitaxial Films. *Phys. Rev. B* **2000**, *61*, 13659−13669.
(32) Tenne, D. A.; Park, S.; Kampen, T. U.; Das, A.; Scholz, R.; Zahn, D. R. T. Single Crystals of the Organic Semiconductor Perylene Tetracarboxylic Dianhydride Studied by Raman Spectroscopy. *Phys. Rev. B* **2000**, *61*, 14564−14569.
(33) Scholz, R.; Friedrich, M.; Salvan, G.; Kampen, T. U.; Zahn, D. R. T.; Frauenheim, T. Infrared Spectroscopic Study of the Morphology of 3,4,9,10-Perylene Tetracarboxylic Dianhydride Films Grown on H-passivated Si(111). *J. Phys.: Condens. Matter* **2003**, *15*, 2647−2663.
(34) Cerdeira, F.; Garriga, M.; Alonso, M. I.; Osso, J. O.; Schreiber, F.; Dosch, H.; Cardona, M. Raman Spectroscopy as a Probe of Molecular Order, Orientation, and Stacking of Fluorinated Copper-Phthalocyanine (F16CuPc) Thin Films. *J. Raman Spectrosc.* **2013**, *44*, 597−607.
(35) Breuer, T.; Celik, M. A.; Jakob, P.; Tonner, R.; Witte, G. Vibrational Davydov Splittings and Collective Mode Polarizations in Oriented Organic Semiconductor Crystals. *J. Phys. Chem. C* **2012**, *116*, 14491−14503.
(36) Petelenz, B.; Petelenz, P.; Shurvell, H. F.; Smith, V. H. Reconsideration of the Electroabsorption Spectra of the Tetracene and Pentacene Crystals. *Chem. Phys.* **1988**, *119*, 25−39.
(37) Ambrosch-Draxl, C.; Nabok, D.; Puschnig, P.; Meisenbichler, C. The Role of Polymorphism in Organic Thin Films: Oligoacenes Investigated from First Principles. *New J. Phys.* **2009**, *11*, 125010.
(38) Tavazzi, S.; Raimondo, L.; Silvestri, L.; Spearman, P.; Camposeo, A.; Polo, M.; Pisignano, D. Dielectric Tensor of Tetracene Single Crystals: The Effect of Anisotropy on Polarized Absorption and Emission Spectra. *J. Chem. Phys.* **2008**, *128*, 154709.

(39) Yamagata, H.; Norton, J.; Hontz, E.; Olivier, Y.; Beljonne, D.; Bredas, J. L.; Silbey, R. J.; Spano, F. C. The Nature of Singlet Excitons in Oligoacene Molecular Crystals. *J. Chem. Phys.* **2011**, *134*, 204703.
(40) Beljonne, D.; Yamagata, H.; Bredas, J. L.; Spano, F. C.; Olivier, Y. Charge-Transfer Excitations Steer the Davydov Splitting and Mediate Singlet Exciton Fission in Pentacene. *Phys. Rev. Lett.* **2013**, *110*, 226402.
(41) Fritz, S. E.; Martin, S. M.; Frisbie, C. D.; Ward, M. D.; Toney, M. F. Structural Characterization of a Pentacene Monolayer on an Amorphous SiO_2 Substrate with Grazing Incidence X-ray Diffraction. *J. Am. Chem. Soc.* **2004**, *126*, 4084−4085.
(42) Brillante, A.; Bilotti, I.; Della Valle, R. G.; Venuti, E.; Girlando, A.; Masino, M.; Liscio, F.; Milita, S.; Albonetti, C.; D'Angelo, P.; et al. Structure and Dynamics of Pentacene on SiO_2: From Monolayer to Bulk Structure. *Phys. Rev. B* **2012**, *85*, 195308.
(43) Drummy, L. F.; Martin, D. C. Thickness-Driven Orthorhombic to Triclinic Phase Transformation in Pentacene Thin Films. *Adv. Mater.* **2005**, *17*, 903−907.
(44) Mattheus, C. C.; Dros, A. B.; Baas, J.; Meetsma, A.; de Boer, J. L.; Palstra, T. T. M. Polymorphism in Pentacene. *Acta Crystallogr., Sect. C: Cryst. Struct. Commun.* **2001**, *57*, 939−941.
(45) Schiefer, S.; Huth, M.; Dobrinevski, A.; Nickel, B. Determination of the Crystal Structure of Substrate-induced Pentacene Polymorphs in Fiber Structured Thin Films. *J. Am. Chem. Soc.* **2007**, *129*, 10316−10317.